Acta Oceanol. Sin., 2018, Vol. 37, No. 5, P. 39–46
DOI: 10.1007/s13131-018-1209-1
http://www.hyxb.org.cn
E-mail: hyxbe@263.net

Time correction of the ocean bottom seismometers deployed at the southwest Indian ridge using ambient noise cross-correlation

LIU Yunlong[1, 2], LIU Cai[1], TAO Chunhui[1, 2]*, YAO Huajian[3], QIU Lei[2], WANG Ao[2, 4], RUAN Aiguo[2], WANG Hanchuang[2], ZHOU Jianping[2], LI Huaiming[2], DONG Chuanwan[2, 5]

[1] College of Geoexploration Science and Technology, Jilin University, Changchun 130026, China

[2] Key Laboratory of Submarine Geosciences, Second Institute of Oceanography, State Oceanic Administration, Hangzhou 310012, China

[3] Laboratory of Seismology and Physics of Earth's Interior, School of Earth and Space Sciences, University of Science and Technology of China, Hefei 230026, China

[4] Institute of Geophysics and Geomatics, China University of Geosciences, Wuhan 430074, China

[5] School of Earth Sciences, Zhejiang University, Hangzhou 310027, China

Received 7 September 2017; accepted 3 January 2018

Abstract

Seismic monitoring using ocean bottom seismometers (OBS) is an efficient method for investigating earthquakes in mid-ocean ridge far away from land. Clock synchronization among the OBSs is difficult without direct communication because electromagnetic signals cannot propagate efficiently in water. Time correction can be estimated through global positioning system (GPS) synchronization if clock drift is linear before and after the deployment. However, some OBSs in the experiments at the southwest Indian ridge (SWIR) on the Chinese DY125-34 cruise had not been re-synchronized from GPS after recovery. So we attempted to estimate clock drift between each station pairs using time symmetry analysis (TSA) based on ambient noise cross-correlation. We tested the feasibility of the TSA method by analyzing daily noise cross-correlation functions (NCFs) that extract from the data of another OBS experiment on the Chinese DY125-40 cruise with known clock drift and the same deployment site. The results suggest that the NCFs' travel time of surface wave between any two stations are symmetrical and have an opposite growing direction with the date. The influence of different band-pass filters, different components and different normalized methods was discussed. The TSA method appeared to be optimal for the hydrophone data within the period band of 2–5 s in dozens of km-scale interstation distances. A significant clock drift of ~2 s was estimated between OBSs sets through linear regression during a 108-d deployment on the Chinese cruise DY125-34. Time correction of the OBS by the ambient noise cross-correlation was demonstrated as a practical approach with the appropriate parameters in case of no GPS re-synchronization.

Key words: clock drift, cross-correlation, ambient noise, OBS

Citation: Liu Yunlong, Liu Cai, Tao Chunhui, Yao Huajian, Qiu Lei, Wang Ao, Ruan Aiguo, Wang Hanchuang, Zhou Jianping, Li Huaiming, Dong Chuanwan. 2018. Time correction of the ocean bottom seismometers deployed at the southwest Indian ridge using ambient noise cross-correlation. Acta Oceanologica Sinica, 37(5): 39–46, doi: 10.1007/s13131-018-1209-1

1 Introduction

Hydrothermal fields at mid-ocean ridges are active areas of magma and tectonics with frequent induced seismic activity. Most of this activity is low magnitude earthquakes that cannot be detected by seismic stations on land. Our study area, the Dragon Horn field (e.g., Tao et al., 2012, 2014) is located at 49.6°E on the Southwest Indian Ridge, which is more than 2 000 km far from the adjacent African continent to the north and Antarctica to the south. Ocean bottom seismometer (OBS) monitoring systems are thus necessary to explore the microearthquakes related to magmatism in the hydrothermal environment. Previously, a single OBS developed near the Longqi hydrothermal vents recorded thousands of earthquakes with a small magnitude (M_L<3) (Liu et al., 2018). In order to improve the accuracy of the epicenter measurements, our group conducted experiments with OBS arrays during the cruises CDC 34th and 40th (hereinafter referred to as CDC 34th and 40th of Chinese DY125-34 and DY125-40 cruises).

Time synchronization must be considered when processing seismic data. Clock drift between OBS arrays is common because OBSs do not have real-time synchronization with GPS, which is in contrast to onshore monitoring stations. Generally, an internal clock with a crystal oscillator reckons an OBS recording. The frequency of the crystal oscillator can be changed depending on its environments with regards to temperature and pressure (Gardner and Collins, 2012). Moreover, such clock drift can accumulate up to several seconds for a long observation. Application of the double-difference technique to the relocation of microearthquakes near the Longqi hydrothermal vents requires accuracy of tens of meters in order to study the hydrothermal circula-

Foundation item: China Ocean Mineral Resources R & D Association Major Project under contract No. DY135-S1-01; the National Natural Science Foundation of China under contract Nos 41506078, 41706042 and 41522404; the Basic Research Foundation of Second Institute of Oceanography, SOA under contract No. JG0608.
*Corresponding author, E-mail: taochunhuimail@163.com

tion and detachment faults where microearthquakes are concentrated (e.g., Stroup et al., 2009; Pontbriand and Sohn, 2014; Schlindwein and Schmid, 2016). Therefore, suitable correction of clock drift is necessary for the location of earthquakes with high-precision and tomographic inversion of velocity structure (Gouedard et al., 2014). The instrument clock can be synchronized to a GPS time prior to a typical OBS deployment, and the offset from GPS time is measured immediately after recovery, which allows a linear drift to be removed from the dataset. However, in the processing of recycled OBS in CDC 34th, GPS resynchronization was unsound, and clock drift could not be corrected. Hence, we use noise cross-correlation to synchronize the clocks between station pairs among an array of OBSs based on the continuous recording of ambient noise (e.g., Sabra et al., 2005; Stehly et al., 2007; Sens-Schönfelder, 2008; Gouedard et al., 2014).

The technique of retrieving surface wave Green functions by ambient noise cross-correlation is used to obtain group or phase velocity for ambient noise tomography (e.g., Shapiro et al., 2005; Yao et al., 2006, 2011), as well as to correct the time error of the stations and measure the time variation of clock drift with the date (e.g., Stehly et al., 2007; Sens-Schönfelder, 2008; Gouedard et al., 2014). The possibility of using the oceanic ambient noise cross-correlation function to estimate the time offset between two hydrophone arrays with a large value of 35 s was confirmed by Sabra et al. (2005). Stehly et al. (2007) separated time shifts associated with instrumental clock drift from the Green's function by observing the evolution of surface-wave travel times over approximately 11 years of continuous recordings. The accuracy of this method was proposed by Sens-Schönfelder (2008) to exceed the precision of the internal station clocks after only a single day of uncorrected drift. It was later applied by Hannemannn et al. (2014) to synchronize clocks of a deep water OBS arrays with a 75 km aperture, which showed that the linear drift was visible in the correlation results of the vertical components and the hydrophone. Gouedard et al. (2014) presented two techniques to retrieve clock drift between OBSs that is the time symmetry analysis (TSA) method and the virtual doublet analysis method, and discussed their advantages and drawbacks. For a fully isotropic noise source, TSA has a superior resolution over a long time scale.

In our experiments, two OBS arrays were developed in the Dragon Horn area at different cruises (CDC 34th and CDC 40th). We tested the feasibility of TSA for ambient noise cross-correlation using CDC 40th dataset with known clock drift. Here we used 37-d continuous records to extract the surface wave part of the Green's function. Time variation of symmetry of the noise cross-correlation functions (NCFs) using different components, time window duration and period bands were discussed in order to select the best parameter for achieving the recovery of the Green's function from ambient noise (Campillo, 2006). Furthermore, we applied these parameters to measure relative clock drift between the OBSs of CDC 34th by the same method. Finally, the relative clock drifts with time between station pair were calculated using the linear form $y=kx+b$.

2 Data and methods

2.1 *Data acquisition*

In 2015, we conducted an OBS experiment during CDC 34th to better interpret the geological processes of hydrothermal circulation in the Longqi field (37.7°S, 49.6°E). Four OBSs with three-component seismometers and a hydrophone were deployed in the 2.5–3.5 km deep water near the Longqi vents from December 2014 to April 2015. As shown in Fig. 1, there were two kinds of OBS: (1) Geopro Sedis IV (60 s–50 Hz) made in Germany; and (2) 1-4C long-period OBS (30 s–50 Hz) developed independently by the Institute of Geology and Geophysics, Chinese Academy of Sciences (Ruan et al., 2010). The longest interval in the OBS array was approximately 20 km. The OBSs recorded seismic data over approximately four month with a sampling rate of 100 Hz for the German devices and 50 Hz for the Chinese ones. During recovery, OBS did not resynchronize from GPS after rising from the water because of instrument malfunction. Therefore the clock drift could not be calibrated by linear regression after resynchronization.

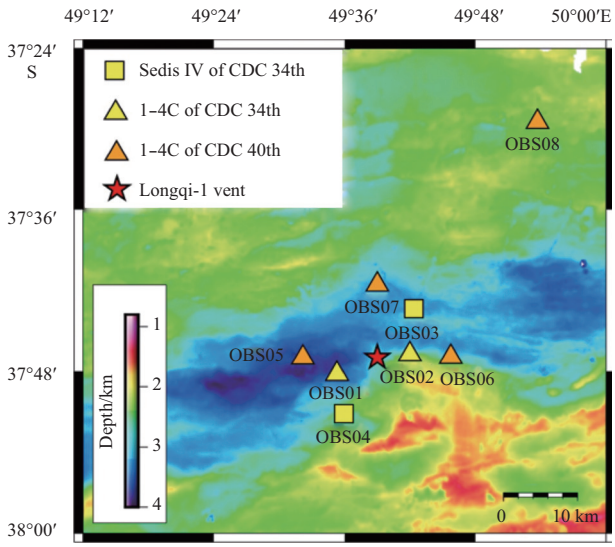

Fig. 1. Bathymetric maps of the Dragon Horn area showing the location of OBSs. Yellow symbols denote the OBSs of CDC 34th (the rectangles are the Sedis IV made in Germany and the triangles the 1-4C made in China), orange triangles the 1-4C OBSs of CDC 40th, and the red star the Longqi-1 hydrothermal vent.

A series of OBS arrays with a larger scale of ~30 km were deployed in the same field in 2016 for a period of 37 days during the CDC 40th. Four of them were used to calculate the clock drift by ambient noise cross-correlation due to the known time shift in clock drift (Fig. 1). The time shift rate of these OBSs was determined by a computed crystal oscillator difference with a range of 2–20 s per year. These large clock drifts cannot be ignored for recording over a long period. The OBSs recording of CDC 40th is used to test the feasibility of the TSA method and the appropriation of different parameters such as the surface wave period band, the instrument component and the duration of the time window.

2.2 *Time symmetry analysis method*

When noise sources are distributed homogeneously, the Green's function of the medium is reconstructed flawlessly, for a pair of stations the surface wave travel time should be symmetrical and not vary with time. In a practice however, the recorded wave-field is not isotropic and the travel time of the NCF is asymmetrical. Three main factors can lead to the asymmetry of NCFs: (1) physical property changes in the medium; (2) temporal variations in the spatial distribution of noise sources; and (3) clock drift of the stations. In our OBS deployment, firstly, variations in crustal velocities are usually negligibly small; secondly, in the

seabed environment, the main noise is the secondary ocean microseisms with a period of ~4 s (Aster et al., 2008) in deep water. We selected the secondary ocean microseisms that are distributed nearly equally in a diffuse field by filtering in a convenient band (Webb et al., 1991; Dolenc et al., 2005), as discussed in the following section. In this way, we assumed the asymmetry of NCF travel time to result from the clock drift among the OBSs.

Based on the above assumptions, we used the TSA method to determine the clock drift of each station pairs. Normally, the clock drift can be decomposed into static clock drift (stationary) and dynamic clock drift (changing in time). A synthetic test to demonstrate how clock drift influences the correlation results in 30 s time windows and how to measure the static and dynamic clock drift respectively is displayed in Fig. 2 (Hannemann et al., 2014). Several wavelets occurring every 30 s starting at 10 s at Trace 1 and 5 s at Trace 2 were used instead of consecutive ambient noise. A time variation clock drift of 1 s per 100 s at Trace 1 was then added (red dashed line in Fig. 2). The cross-correlation method was applied to Trace 1 and Trace 2 in the fixed time window (blue box in Fig. 2). The static clock drift (dt^{stat}) and dynamic clock drift (dt^{dyn}) were measured from zeros-shift of lag time marked in the cross-correlation results. We could then estimate the static clock drift and dynamic clock drift as a sample workflow extract following the method of Gouedard et al. (2014):

(1) For each pair of OBSs, we calculated a daily NCF $s(t)$ consisting of the causal parts from one side and the anti-causal parts coming from the opposite side, denoted as $s^{+}(t)$ and $s^{-}(t)$ and written as

$$\left.\begin{aligned} s\left(t\right) &= s^{-}\left(t\right) + s^{+}\left(t\right). \\ s^{+}\left(t\right) &= 0, t < 0;\ s^{-}\left(t\right) = 0, t > 0. \end{aligned}\right\} \tag{1}$$

(2) The first daily NCF was used as our reference trace $r(t)$ which is decomposed into $r^{+}(t)$ and $r^{-}(t)$, akin to what was described in Eq. (1). The reference trace was correlated with the correlation results of the station pairs at all other dates. The time shift dt^{+} and dt^{-} for the positive and negative sides were measured by selecting the lag time for the maximum cross-correlations $r^{+}\left(t\right) \otimes s^{+}\left(t\right)$ and $r^{-}\left(t\right) \otimes s^{-}\left(t\right)$, respectively. Then the dynamic clock drift was obtained by the difference $dt^{+} - dt^{-}$ as follows:

$$dt^{\mathrm{dyn}} = \frac{dt^{+} - dt^{-}}{2}. \tag{2}$$

(3) Likewise, the static clock drift dt^{stat} was obtained from the cross-correlation $r^{+}\left(t\right) \otimes r^{-}\left(t\right)$ as described in the dynamic clock drift, and finally the absolute clock drift was obtained as

$$dt^{\mathrm{rel}} = dt^{\mathrm{dyn}} + dt^{\mathrm{stat}}. \tag{3}$$

(4) For any three stations A, B and C, the relative clock drifts $dt^{\mathrm{rel}}_{\mathrm{AB}}$, $d^{\mathrm{rel}}_{\mathrm{BC}}$ and $dt^{\mathrm{rel}}_{\mathrm{AC}}$ between each pair must satisfy the closure relation:

$$dt^{\mathrm{rel}}_{\mathrm{AB}} + dt^{\mathrm{rel}}_{\mathrm{BC}} - dt^{\mathrm{rel}}_{\mathrm{AC}} = 0. \tag{4}$$

To help reduce the error in the clock drift, the closure relations between all combinations of the three stations as an additional constraint were considered. Hence, we determined the optimal clock drift of each station pairs at all dates by conjugate gradient methods to find the optimal solution of the linear Eq. (4).

The feasibility of the TSA approach was firstly verified by estimating the clock drift of the OBSs during the survey of CDC 34th with the known clock drift. Secondly, the signal to noise ratio (SNR) of NCFs in the four recording components was estimated and the superior one was selected and cross-correlated. We also analyzed the symmetry of the NCFs in different bands to test which frequency band was appropriate for recovering the Green's function from ambient noise. Furthermore, through observing the time variation of NCFs, the clock drift with date was computed by linear regression and the measurement error was estimated by comparing the estimated drift with the expected one. Finally, we confirmed that the clock drift estimated by ambient noise cross-correlation was good, and applied it to compute

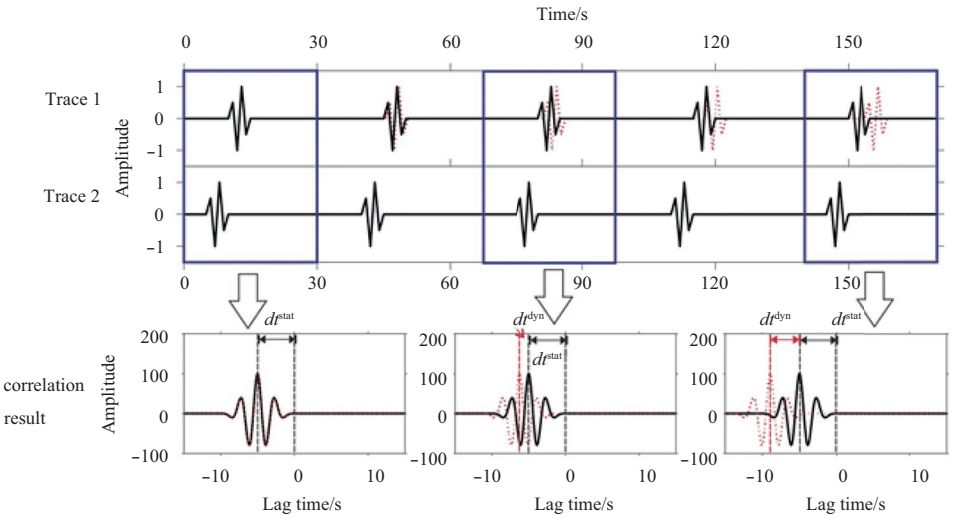

Fig. 2. Schematic plots of generating the clock drifts by a wavelet. The black solid line represents waveforms and their correlation results without time-shift, and the red dashed line waveform with time-shift; dt^{stat} is the static drift, dt^{dyn} the dynamic time-shift, and the total clock drift $dt^{\mathrm{rel}} = dt^{\mathrm{dyn}} + dt^{\mathrm{stat}}$; correlation results between Trace 1 and Trace 2 are given for un-shifted time windows (blue boxes). This figure is modified from Figure 3 in Hannemann et al. (2014).

the clock drift of OBSs on CDC 34th using the appropriate parameters discussed in the next section.

3 Results and discussion

3.1 *Time symmetry of NCFs on CDC 40th*

In this study, we used the TSA method for experiments on CDC 40th. Prior to computing the cross-correlations, several data processing methods were considered for recovering the Green's function of ambient noise and improving the SNR of NCFs.

3.1.1 *Influence of component selection*

The seismic data were cross-correlated between each station pairs in 1-d records to form the daily NCFs following preprocessing of down-sampling, spectrum whitening, amplitude normalization and low frequency band-pass filtering. Figure 3 shows an example of daily NCFs for four components filtered in the period band of 2–5 s at the available pair of OBS05 and OBS07. The hydrophone and vertical seismometer share the symmetry of the daily NCFs. However, by selecting the maximum NCFs (marked by the red dots in Fig. 3), the measured lag time of the horizontal component infrequently shows the level of symmetry expected due to low SNR of the horizontal recordings. To measure the quality of the NCFs results in different components, we calculated the SNR according to the following method: (1) a signal window was selected around the arrival time of the surface wave and the maximum of the absolute value in this time window was found; (2) the mean square deviation of noise signal in the selected window was then computed based on the actual situation; and (3), finally the SNR of the NCFs was defined as

$$SNR = \frac{\max(|S_i|)}{\sqrt{\frac{\sum_{j=1}^{n}(N_j-\bar{N})^2}{n-1}}}, \tag{5}$$

where S_i is the signal sequence of the m length, N_j is the noise sequence of the n length, $\bar{N}$ is the mean of noise sequence, $i = 1, 2, \ldots, m; j = 1, 2, \ldots, n$.

Using the Eq. (5) the SNR of NCFs was calculated for each day and then stacked them to a total of 37 d. We selected 5 s around the surface wave arrival time for signal and 60–80 s of the lag time for noise. The result indicates that the SNR of the stacked NCFs in the hydrophone component is highest at 7.6 and the second highest is the vertical component of 6.0. However, they are relatively low in the other two horizontal components (west-east component and north-south component) at 5.3 and 2.4 respectively. Hannemann et al. (2014) found good agreement in the clock drift behavior between the vertical seismometer and the hydrophone by comparing their correlation results. Furthermore, the hydrophone usually works well and the vertical component is occasionally clamped. Combined with our study results, we used the hydrophone component signal for cross-correlation in the following processing.

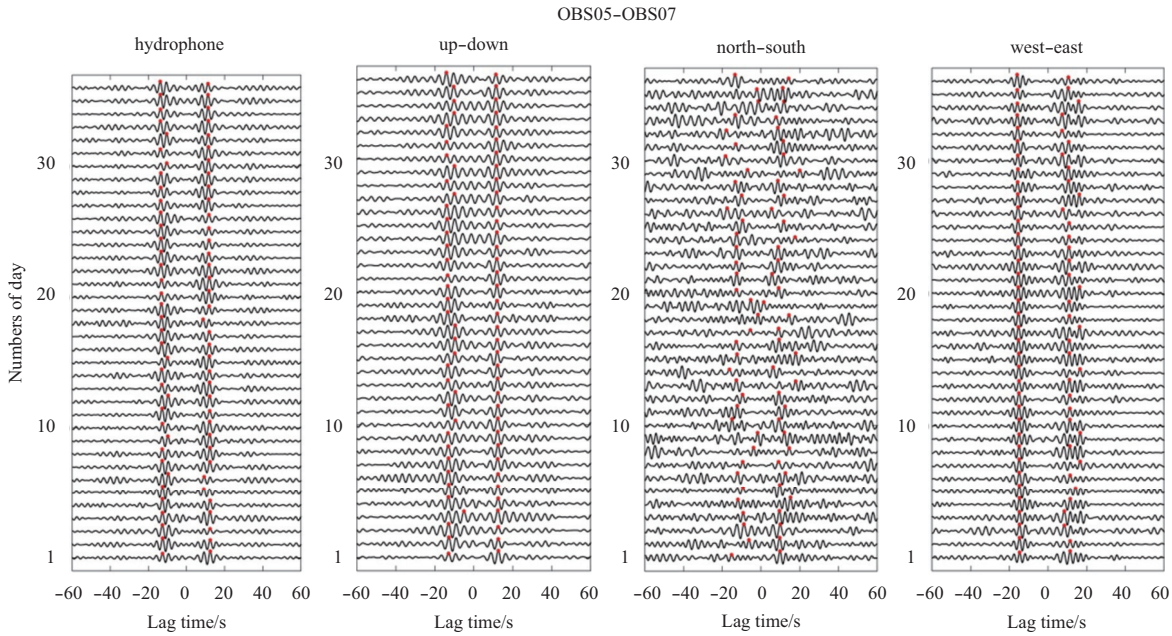

Fig. 3. Daily NCFs at the pair of OBS05-OBS07 in the 2–5 s period band in four components: hydrophone component, up-down component, north-south component and west-east component. Both positive and negative times were selected by the maximum of each daily NCF marked by the red dots.

3.1.2 *Influence of band-pass in different period bands*

The NCFs in several narrow bands (1–2 s, 2–5 s, 5–10 s and 10–20 s) was investigated to determine what part of the period band is usable, as shown in Fig. 4. The daily NCFs of the hydrophone recording between the station pairs in each band were computed. In order to evaluate the SNR of the NCFs in these bands, Eq. (5) was also used to find an appropriate band. The results show that the signal filtered in the 2–5 s band has a higher SNR of 7.2 than those in the other bands (SNR=2.8, 1–2 s; SNR=5.9, 5–10 s; SNR=2.1, 10–20 s) and the symmetry of the NCFs in the band of 2–5 s is superior to the others (Fig. 4).

On the other hand, Bensen et al. (2007) summarized the empirical relation Eq. (6) based on many tests on the recovery of Green's function:

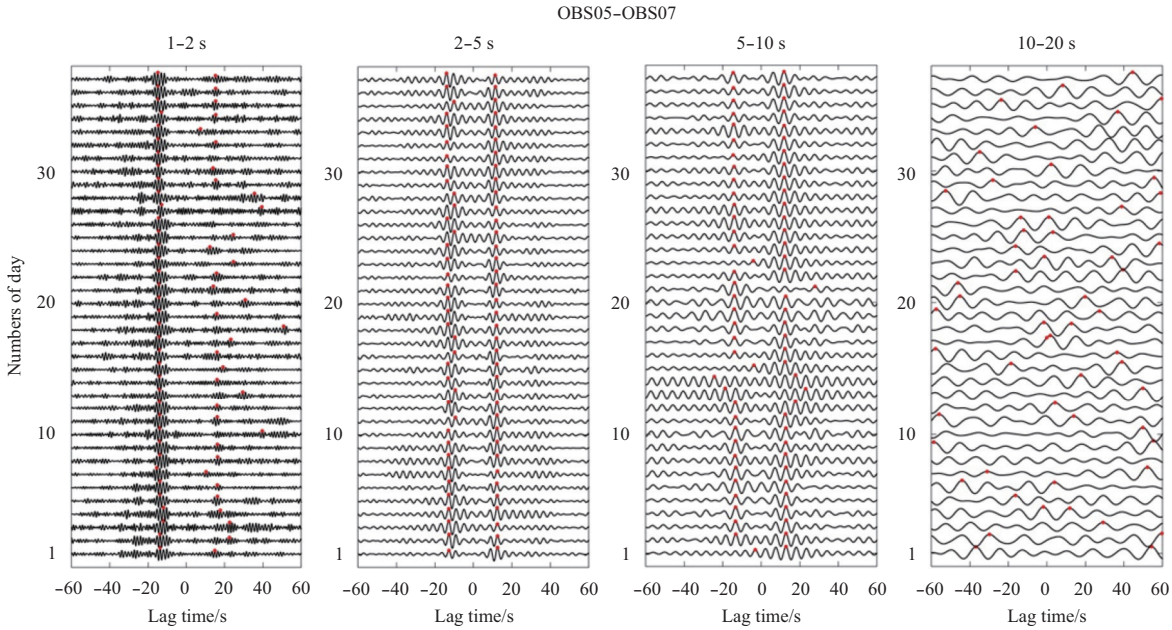

Fig. 4. Daily NCFs for the pair OBS05-OBS07 on the hydrophone components in different period bands: 1–2 s, 2–5 s, 5–10 s, and 10–20 s. Both positive and negative travel times are selected by the maximum of each day NCF marked by the red dots.

$$r \geqslant 3\lambda = 3cT \rightarrow T \leqslant \frac{r}{3c}, \tag{6}$$

where r is the interstation distances, λ is the wavelength, c is the surface wave phase velocity, and T is the selected period. This means that the longest period of the recovered Green's function from ambient noise recorded by the two stations should be less than one third of the ratio of station spacing to phase speed. The longest period adopted was 5 s because of the greatest interstation distance of 30 km and a surface wave velocity of 2 km/s. Additionally, the SNR of cross-correlation results of the signal filtered in 2–5 s is the highest, thus we used this period band as an appropriate parameter in the processing of NCFs.

3.1.3 *Time variation of NCFs*

The fluctuation of the NCFs following the time variation using 37-d records on the hydrophone component filtered in the period band of 2–5 s was analyzed. We also computed clock drift, based on the time delay measurements. Before obtaining NCFs between every two station pairs, preprocessing was necessary as described in details by Bensen et al. (2007). These include removal of instrument response, resampling, removal of mean and trend, band-pass filter, temporal normalization and spectrum whiting. Specifically, amplitude normalization in the time domain was necessary because the surface wave travel time of NCFs is influenced by large earthquakes and any unstable noise sources near the station. The two normalization methods are one-bit and running-average. The latter is widely used to remove the earthquakes effect and air gun signals during the experiments to improve the SNR (Larose et al., 2004). We compared the two methods by computing the SNR of NCFs as Eq. (5). The SNR results using a running average were a little higher than for the one-bit method. Hence, we used the normalization method of the running average in our study. Additionally, we assume the instrument response is the same for the same kind of OBS and so the influence from the removal of instrument response is limited.

Six pairs of daily NCFs among the four OBSs are shown in Fig. 5. We observed a clear linear trend for the NCFs with date, which indicates the influence of dynamic clock drift between OBSs. For example, amplitude in the positive and the negative parts between the OBS05 and OBS06 is different, which may be due to inhomogeneous illumination of noise sources (Stehly et al., 2006), but the positive and negative times are symmetrical and change with time. Stehly et al. (2007) proposed that the clock drift between the two stations would produce a time-shift of NCFs resulting in a longer travel time in the positive time and a shorter travel time in the negative time or vice versa and their differences would remain the same by observing evolution of cross-correlation results with date.

To confirm that the linear variation in the positive and negative time is almost exclusively affected by clock drift, we tested cross-correlation results of different length for one day, two day and five day (Fig. 6). The time shifts satisfied the linear regression between the start and the end of the experiment and the dynamic clock drift can be obtained by the slope of the date. Table 1 shows variation rate of the dynamic clock drift per day measured by the time shift of NCFs of one day, two days and five days using linear regression. The theoretical dynamic clock drifts in Table 1 were obtained by the computed crystal oscillator difference of the instrument. Compared with the standard frequency of a crystal oscillator (12 288 000 Hz), the instruments began with a variance recorded in the log file because of the temperature and pressure influence of the surrounding environment. We used a simple relationship in Eq. (7) to compute the theoretical dynamic drift per day:

$$dt_{ij}^{\text{the}} = \frac{PClk_i - PClk_j}{12\ 288\ 000} \times 24 \times 3\ 600, \tag{7}$$

where $PClk_i$ and $PClk_j$ are the vibration frequency of crystal oscillator of the ith and jth OBS respectively; i, j=1, 2, 3, 4 represent the number of the OBS.

The clock drift rates of different day lengths were almost identical (Table 1). The largest error was 0.003 4 s per day. Therefore the NCF time shifts that changed linearly with date in Fig. 5

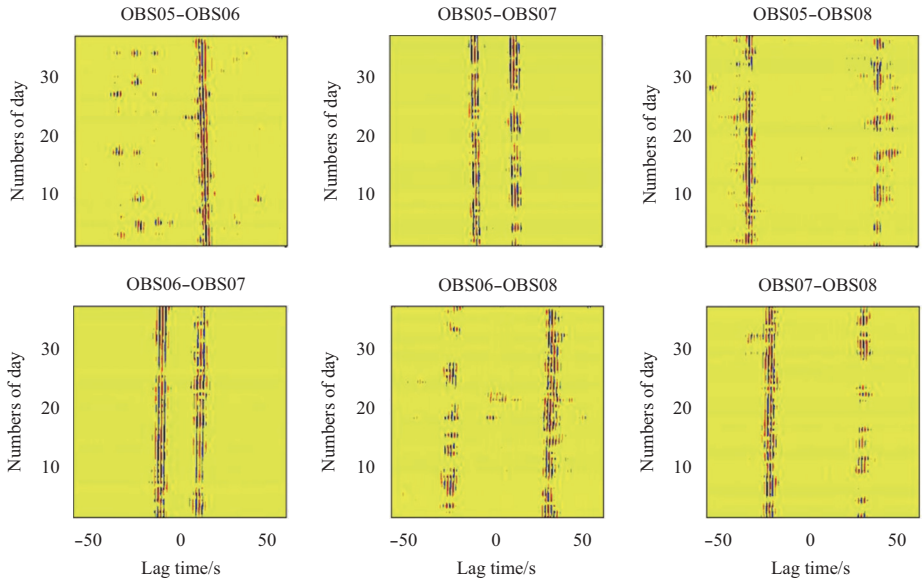

Fig. 5. Daily NCFs on the hydrophone component in the band of 2–5 s between each pair of the four stations. The window of lag time ranges from –60 s to 60 s, which is enough for the surface-wave arrival time in this case.

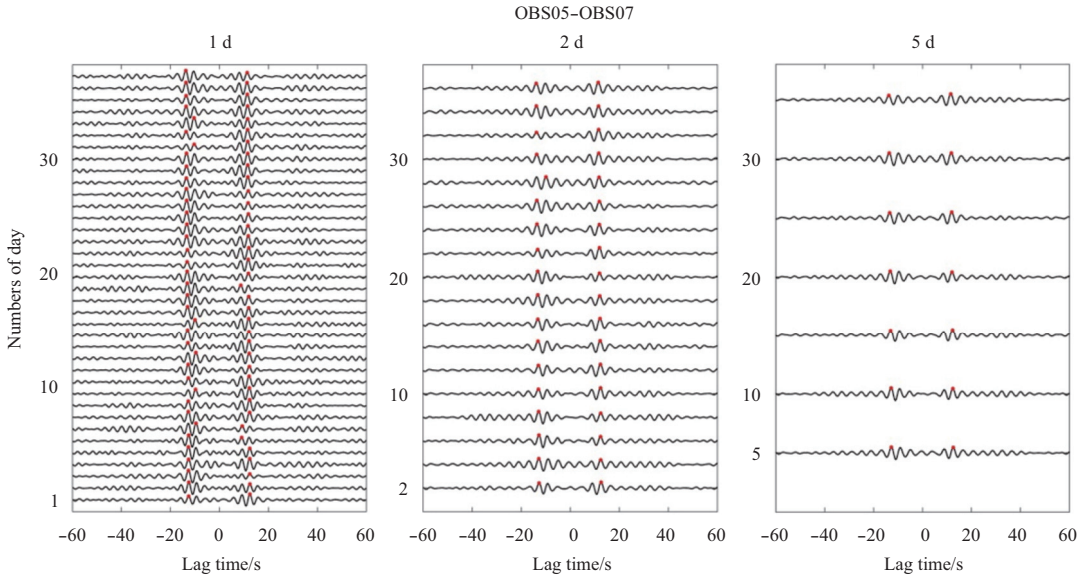

Fig. 6. NCFs of one day, two days and five days at the pair of OBS05-OBS07 on the hydrophone components filtered in the band of 2–5 s. Both positive and negative times are indicated by the maximum of NCFs marked by the red dots.

results from the influence of the dynamic clock drift between stations. Meanwhile, the dynamic shift due to a change in the spatial distribution of the noise source was expected to decrease when increasing the length of the correlated time-series. This was because of the improved spatial homogenization of the noise for a longer time. Concurrently, the time resolutions of the longer time become lower. In our cross-correlation results, symmetry of the NCFs was good and only slightly affected by the temporal variations in source distribution. Therefore we utilized the time series of one day for the time window of cross-correlation in this paper.

3.1.4 *Estimation of time error between the estimated and theoretical values*

In this experiment, a reference trace is defined as the first day of the deployment and the start time of all stations is synchronized through GPS so there is no static clock error between the stations and the dynamic clock drift represents the whole clock drift. We found small errors in the dynamic clock drift per day of our estimates and good agreement with that of the theoretical values for the majority of the stations (Table 1). The standard deviation of the difference between the estimated relative clock drift and the theoretical value of the OBS pair was computed using the following equation:

$$\sigma = \sqrt{\frac{1}{N}\sum_{n=1}^{N}\left(dt^{\mathrm{dyn}} - dt^{\mathrm{the}}\right)^2}, \tag{8}$$

where dt^{dyn} is the dynamic relative clock drift and dt^{the} is the the-

Table 1. The dynamic clock drift estimated using the different length data

Station pairs	Dynamic clock drift rate per day/s·d^{-1}			
	Theoretical	NCFs of one day	NCFs of two days	NCFs of five days
OBS05-OBS06	0.073 8	0.066 9	0.066 1	0.067 0
OBS05-OBS07	0.032 3	0.032 9	0.032 8	0.033 0
OBS05-OBS08	–0.007 1	–0.002 1	–0.000 8	–0.001 1
OBS06-OBS07	–0.041 5	–0.038 2	–0.038 5	–0.038 4
OBS06-OBS08	–0.080 9	–0.080 5	–0.079 9	–0.080 0
OBS07-OBS08	–0.039 4	–0.040 7	–0.043 5	–0.044 1

oretical relative clock drift measured by the frequency of the crystal oscillator. N is the day length of deployment.

Figure 7 illustrates the measurement of the dynamic clock drift for OBSs related to the reference station OBS05. The standard deviation errors between the estimated clock drift and the expected value for each pairs are 0.128 s for OBS06, 0.070 5 s for OBS07 and 0.150 1 s for OBS08 respectively.

3.2 *Application of TSA on the CDC 40th*

As discussed above, the TSA method of ambient noise with suitable parameters was applied successfully to the measurement of clock drift on the CDC 40th. The results confirm that the difference between the estimated value and the theoretical value is small enough to correct our clock drift using this method. The same process was applied to the clock drift of OBSs on CDC 34th with the relatively greater time drift because of a longer observation. The preprocessing for the NCF computing was as above, and the hydrophone time series of one day with the period band 2–5 s was selected in this experiment.

For each pairs of stations, the positive time dt^+ and negative time dt^- of the NCFs were evaluated to the same direction symmetrically. The dynamic relative drift with respect to the reference trace was obtained by Eq. (2) on the assumption of linear regression. Static drift was a large difference of every two OBSs because several instruments began with a static clock offset from GPS and a different deployment time. Thus the total clock drifts were estimated by the following linear fitting equation:

$$dt_n^{\mathrm{rel}} = K\,(n-1) + B\,, \tag{9}$$

where K is the slope of the dynamic clock drift, B is the static clock drift that is constant over time, and n=1, 2, 3, ..., 108 is the number of day.

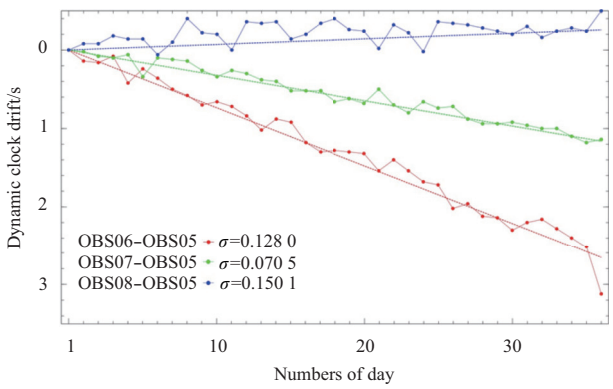

Fig. 7. Time variation of clock drifts using TSA for three OBSs relative to OBS05 with date. The dashed lines represent the expected value of time drift for comparison with the estimated one.

Additionally, compared with estimation of the dynamic clock drift the static clock drift is inaccurate because the positive and negative parts of the NCF for the first day as the reference trace are not constantly similar. To determine the static offset to a high precision we used the cross-correlation of $r^+(t) \otimes r^-(t)$, where the reference trace is rebuilt by the stack of all NCFs over the period of the experiments after dynamic clock drift. Figure 8 illustrates that the symmetry of the stacked NCFs is perfectly related to the daily NCF. This is due to sufficient averaging and, possibly, an increased influence of an isotropic source exemplified by a reference trace stacked by all the NCFs of OBS01 and OBS03.

Finally, the total clock drift consisting of the static and dynamic drift is present as in Eq. (9) for each station pair. In order to reduce the estimated error and improve OBS precision, we utilized a conjugate gradient algorithm to determine the optimal results of all stations based on the relation of interstation clock drifts described by Eq. (4). Figure 9 shows that the final clock drift results of the OBSs related to OBS01 as a reference station, as well as linear fitting of the clock drift with the root mean square errors calculated by Eq. (8) where the dt^{exp} is the linear expected result. The standard deviation estimated using TSA are 0.062 5 s, 0.080 6 s and 0.094 5 s for the OBS02-OBS01, OBS03-OBS01, and OBS04-

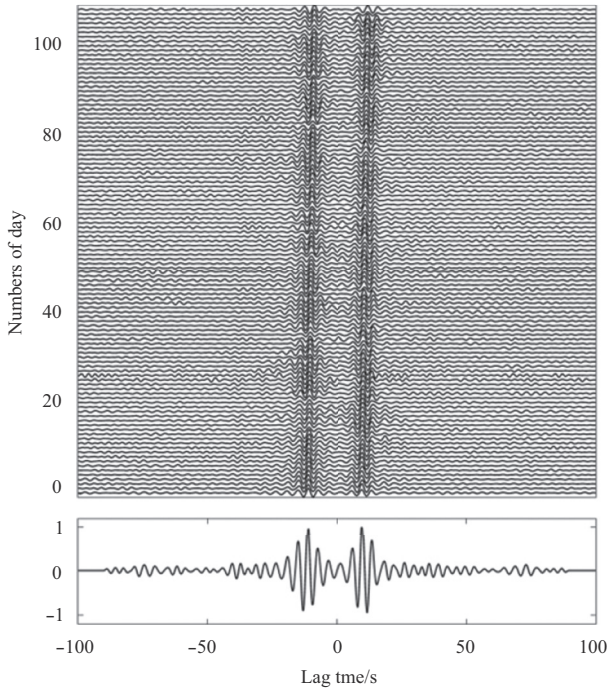

Fig. 8. An example of reference trace of a stack of 108 d NCFs over lag time ranging from –100 s to 100 s using the hydrophone component of OBS01 and OBS03 in the 2–5 s period band on CDC 34th.

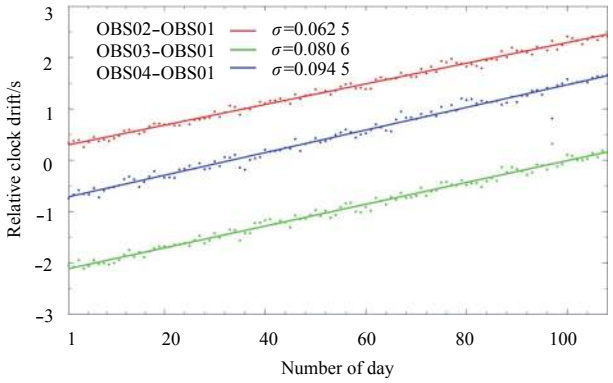

Fig. 9. The relative clock drifts of the OBSs related to OBS01 as a reference station using TSA. The oblique line is the line of best fit; the standard deviation (s) of each pair is shown on the top left.

OBS01, respectively. Although the estimated clock drift is the related value of all stations, it is adequate for correcting time consistently in the same OBS array. The largest relative clock drift accumulated between two OBSs was approximately 2.2 s. This means that research on earthquake location and tomography using the arrival time of the data will improve in accuracy by an order of magnitude.

4 Summary and conclusions

A visible linear clock drift with date was found for the NCFs in the experiments of the OBSs deployed on both CDC 34th and 40th. Using a 1-d series recorded by the hydrophone component filtered to the 2–5 s period bands, we verified that the symmetry of NCFs is nearly perfect with a high SNR. The influence of amplitude normalization using the one-bit and running average methods was almost identical. We evaluated the feasibility of these parameters on the CDC 40th because the clock drift of the OBSs was known. We then applied the same parameters successfully to the OBSs on the CDC 34th. Additionally, the precision of the static drift was improved using the stacked reference trace of all dates. We further optimized the clock drift of all the stations based on the interstation relationship. In the end, the clock drift between every two OBSs was estimated by linear regressions with small deviations. After the 108 d accumulation, the largest relative clock drift exceed non-negligible level of 2 s. Thus time correction is necessary for a long term seismic observation.

In this paper, we confirmed that OBS clock drift, including the static and dynamic offsets could be estimated using TSA techniques with appropriate parameters based on ambient noise cross-correlation. In the deep-sea environment the low frequency secondary ocean microseism are taken as nearly homogeneous noise sources and the time shift of the NCFs results solely from the clock drift between each OBS pair. Hence, using the low frequent noise cross-correction technique can be particularly useful for the OBS data, especially in cases where OBSs malfunction or there is non-linear drift.

Acknowledgements

The authors thank the captain and the crew of CDC 34th and 40th for their efforts to complete the development of the OBSs.

References

Aster R C, McNamara D E, Bromirski P D. 2008. Multidecadal climate-induced variability in microseisms. Seismol Res Lett, 79(2): 194–202

Bensen G D, Ritzwoller M H, Barmin M P, et al. 2007. Processing seismic ambient noise data to obtain reliable broad-band surface wave dispersion measurements. Geophys J Int, 169(3): 1239–1260

Campillo M. 2006. Phase and correlation in 'random' seismic fields and the reconstruction of the Green function. Pure Appl Geophys, 163(2–3): 475–502

Dolenc D, Romanowicz B, Stakes D, et al. 2005. Observations of infragravity waves at the Monterey ocean bottom broadband station (MOBB). Geochem Geophys Geosyst, 6(9): Q09002

Gardner A T, Collins J A. 2012. Advancements in high-performance timing for long term underwater experiments: A comparison of chip scale atomic clocks to traditional microprocessor-compensated crystal oscillators. In: IEEE Oceans. Hampton Roads, VA, USA: IEEE, doi: 10.1109/OCEANS.2012.6404847

Gouedard P, Seher T, McGuire J J, et al. 2014. Correction of ocean-bottom seismometer instrumental clock errors using ambient seismic noise. Bull Seismol Soc Am, 104(3): 1276–1288

Hannemann K, Kruger F, Dahm T. 2014. Measuring of clock drift rates and static time offsets of ocean bottom stations by means of ambient noise. Geophys J Int, 196(2): 1034–1042

Larose E, Derode A, Campillo M, et al. 2004. Imaging from one-bit correlations of wideband diffuse wave fields. J Appl Phys, 95(12): 8393–8399

Liu Yunlong, Tao Chunhui, Liu Cai, et al. 2018. Seismic activity recorded by a single OBS/H near the active Longqi hydrothermal vent at the ultraslow spreading Southwest Indian Ridge (49°39′E). Mar Geores Geotechnol: doi: 10.1080/1064119X.2017.1420114

Pontbriand C W, Sohn R A. 2014. Microearthquake evidence for reaction-driven cracking within the Trans-Atlantic Geotraverse active hydrothermal deposit. J Geophys Res: Solid Earth, 119(2): 822–839

Ruan Aiguo, Li Jiabiao, Chen Yongshun, et al. 2010. The experiment of broad band 1–4C type OBS in the Southwest Indian Ridge. Chin J Geophys (in Chinese), 53(4): 1015–1018

Sabra K G, Roux P, Thode A M, et al. 2005. Using ocean ambient noise for array self-localization and self-synchronization. IEEE J Ocean Eng, 30(2): 338–347

Schlindwein V, Schmid F. 2016. Mid-ocean-ridge seismicity reveals extreme types of ocean lithosphere. Nature, 535(7611): 276–279

Sens-Schönfelder C. 2008. Synchronizing seismic networks with ambient noise. Geophys J Int, 174(3): 966–970

Shapiro N M, Campillo M, Stehly L, et al. 2005. High-resolution surface-wave tomography from ambient seismic noise. Science, 307(5715): 1615–1618

Stehly L, Campillo M, Shapiro N M, et al. 2006. A study of the seismic noise from its long-range correlation properties. J Geophys Res: Solid Earth, 111(B10): B10306

Stehly L, Campillo M, Shapiro N M. 2007. Traveltime measurements from noise correlation: stability and detection of instrumental time-shifts. Geophys J Int, 171(1): 223–230

Stroup D F, Tolstoy M, Crone T J, et al. 2009. Systematic along-axis tidal triggering of microearthquakes observed at 9°50′N East Pacific Rise. Geophys Res Lett, 36(18): L18302

Tao Chunhui, Li Huaiming, Jin Xiaobing, et al. 2014. Seafloor hydrothermal activity and polymetallic sulfide exploration on the southwest Indian ridge. Chin Sci Bull, 59(19): 2266–2276

Tao Chunhui, Lin Jian, Guo Shiqin, et al. 2012. First active hydrothermal vents on an ultraslow-spreading center: Southwest Indian Ridge. Geology, 40(1): 47–50

Webb S C, Zhang Xin, Crawford W. 1991. Infragravity waves in the deep ocean. J Geophys Res, 96(C2): 2723–2736

Yao Huajian, Van Der Hilst R D, De Hoop M V. 2006. Surface-wave array tomography in SE Tibet from ambient seismic noise and two-station analysis: I. Phase velocity maps. Geophys J Int, 166(2): 732–744

Yao Huajian, Gouédard P, Collins J A, et al. 2011. Structure of young East Pacific Rise lithosphere from ambient noise correlation analysis of fundamental- and higher-mode Scholte-Rayleigh waves. Comptes Rendus Geosci, 343(8–9): 571–583